Discrete-time Frequency-shaped Sliding Mode Control for Audio-vibration Rejection in Hard Disk Drives

Minghui Zheng, Xu Chen, and Masayoshi Tomizuka

Mechanical Engineering

University of California, Berkeley

December 2014

Abstract

In this report, a discrete-time frequency-shaped sliding mode control (FSSMC) is proposed for audio-vibration rejection in Hard Disk Drives (HDDs). Such vibrations cause significant degradation of the servo performance and have become a major concern in the HDD industry. The proposed FSSMC involves the frequency-shaped sliding surface design based on peak filters, aiming to provide frequency dependent control allocation in sliding mode control (SMC). Compared to standard SMC, FSSMC provides additional design flexibilities in the frequency domain, and improves vibration rejection during track-following in HDDs. Those benefits are validated by simulation based on benchmark models and actual vibration data.

Contents

1 Introduction

In hard disk drives (HDDs), the increase of data track density necessitates to reduce the position error signal (PES) and improve the servo performance. Sophisticated algorithms have been proposed to control the transient during the track-seeking process. One current challenge for steady-state performance improvement comes from high-frequency vibrations, which may even excite system resonances. Nowadays audio vibrations have become one of the most important vibrations to deal with. They are induced by audio sounds when HDDs are equipped in modern multimedia personal computers.

Sliding mode control has been applied to HDD systems due to its fast convergence and good robustness to unknown disturbance. Lee et al. (2000) applied sliding mode control algorithm to HDDs and achieved fast track-seeking performances. Zhang and Guo (2000) proposed a time-optimal sliding mode control algorithm with a time-varying sliding surface and realized smooth transition from the track-seeking process to the track-following process. Zhou et al. (2001) improved the algorithm to further reduce the settling time during track-seeking. Hu et al. (2009) also proposed a sliding mode control for HDDs based on a time-optimal sliding surface and improved both the transient performance and the steady-state performance. Sliding mode control has been considered as a promising technique for HDDs.

Aiming to extend the design of sliding mode control from time domain to frequency domain, motivated by the frequency-shaped linear quadratic regulator (LQR), Young and Ozguner (1993) proposed frequency-shaped sliding mode control (FSSMC) with a new switching plane and applied it to a flexible robot manipulator. Many authors then extended, improved and applied frequency-shaped sliding mode control to different areas. Nonami et al. (1996) designed a FSSMC based on H_∞ and μ synthesis theory for a flexible arm. Moura et al. (1997) provided a conventional sliding surface that can be made equivalent to the frequency-shaped one, and applied FSSMC to a single degree of freedom robot with a flexible appendage. Yanada and Ohnishi (1999) added a low-pass filter to the control input to suppress chatter in SMC. Koshkouei and Zinober (2000) discussed the design of the frequency-shaped sliding surface based on LQR weighting functions to improve the transient performance. Wu and Liu (2005) designed a FSSMC with an inverse notch filter to control the flying height of the pickup head in optical disk dives. Mehta and Bandyopadhyay (2009) designed a FSSMC based on output sampled measurements to damp the vibration amplitude of a smart beam at its resonance frequencies.

In most of the aforementioned literature, FSSMC is motivated by the frequency-shaped LQR control problem with frequency-varying weighting functions, aiming to attenuate the excitation of undesired system dynamics and enhance the robustness. In this report, the proposed FSSMC is directly motivated by performance enhancement. Specifically, to have customized control allocation for attenuating the large spectral peaks in audio vibrations, the proposed FSSMC increases the 'local gain' of sliding mode control at the frequencies where the servo performance is degraded by audio vibrations. Peak filters are utilized for significant performance improvement of audio-vibration rejection. It is proved that, for

2

the proposed second-order peak filters, as long as the filter poles and zeros are stable, the sliding surface and the full closed-loop system will be stable. For higher-order filter design, the stability condition is more involved (although there are still strong design flexibility). Analysis based on root locus is provided for intuitive design and easy stability analysis. Control algorithms and filter design are provided in discrete-time, whose analysis is more complex than the continuous-time case, but is directly implementable on actual HDDs.

The remainder of the report is organized as follows. Section 2 provides the description of HDD model and the frequency-shaped SMC algorithm. Section 3 provides the stability analysis including both the approaching and the sliding phases of SMC. Section 4 provides the details of peak filter design. Simulation results based on the HDD benchmark package by IEEJ (2007) are provided in Section 5. Section 6 concludes the report.

2 Model Description and Controller Design

2.1 Model Description

The control of a practical model for a single-stage HDD plant can be higher than ten, as shown in Figure 1 (HDD benchmark package by IEEJ, 2007). High frequency resonances are usually attenuated by notch filters.
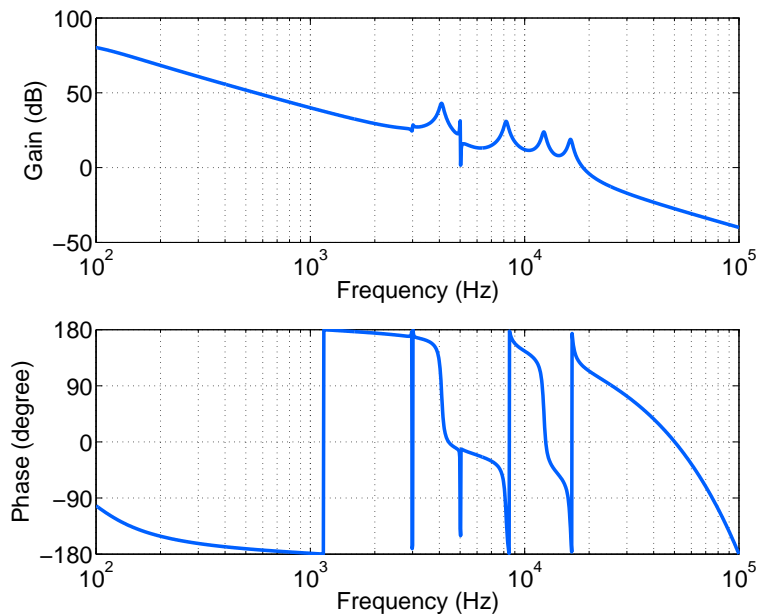

Figure 1: Full Order Model of HDD (IEEJ, 2007)

A double-integrator nominal model that captures the central low-frequency characters is

$$\begin{bmatrix} \dot{y} \\ k_y \dot{v} \end{bmatrix} = \begin{bmatrix} k_y v \\ k_y k_v u \end{bmatrix} \tag{2.1}$$

where u is the actuator input, y is the position of the head in the unit of tracks, v is the velocity, k_v is the acceleration constant, and k_y is the position measurement gain.

Denote $e_1 = y - y_r$, and $e_2 = \dot{e}_1 = k_y v - \dot{y}_r$. In HDD track-following control, $y_r(k)$ and $\dot{y}_r(k)$ are zero. From equation (2.1), the discrete-time error dynamics with unknown bounded disturbance is

$$e(k + 1) = Ae(k) + B(u(k) + d(k)) + B_a v_a(k) \tag{2.2}$$

4

where

$$e(k) = \begin{bmatrix} e_1(k) \\ e_2(k) \end{bmatrix}, A = \begin{bmatrix} 1 & T \\ 0 & 1 \end{bmatrix}, B = \begin{bmatrix} T^2 k_y k_v/2 \\ T k_y k_v \end{bmatrix}, B_a = \begin{bmatrix} 1 \\ 0 \end{bmatrix},$$

T is the sampling time, $|d| \leq D$ is the input force disturbance, and $|v_a| \leq V_a$ is the audio vibrations lumped at the output of the plant.

2.2 Frequency-shaped Sliding Mode Control

In this section, a frequency-shaped sliding mode control (FSSMC) algorithm is proposed to provide enhancements at the frequencies where the servo performance is seriously degraded by large disturbance such as audio vibrations. With this motivation, a peak filter Q_f is introduced to shape sliding surface at the preferred frequencies. Q_f can be regarded as a weighting function to allocate the control effort in the frequency domain: at the frequencies where the weight is large, it is expected that the controller allocates more energy in the input. In this report, the peaks of Q_f are selected at the frequencies where PES is large.

Based on this idea, we have a different definition for the sliding surface in FSSMC, as shown in Figure 2. In traditional definition of sliding surface $s_t(k) = 0$, $s_t(k)$ is defined as $s_t(k) = He(k) = \begin{bmatrix} 1 & h_2 \end{bmatrix} e(k)$ $(h_2 > 0)$. In the frequency-shaped sliding surface $s(k) = 0$, $s(k)$ is modified to

$$s(k) = H \begin{bmatrix} Q_f\{e_1(k)\} \\ e_2(k) \end{bmatrix} = e_f(k) + h_2 e_2(k) \tag{2.3}$$

where e_f is the filtered position error, i.e., $e_f = Q_f\{e_1\}$.

(a) Traditional
Sliding Surface Definition

(b) Frequency-shaped
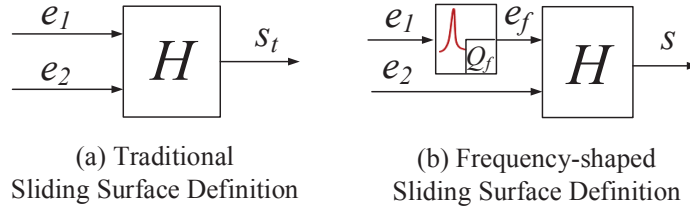Sliding Surface Definition

Figure 2: Sliding Surface Definition

Assume that Q_f has the following state-space realization:

$$\begin{aligned} e_w(k+1) &= A_w e_w(k) + B_w e_1(k) \\ Q_f\{e_1(k)\} &= C_w e_w(k) + D_w e_1(k) \end{aligned} \tag{2.4}$$

Combining equation (2.2) and equation (2.4), the augmented system can be represented as

$$\tilde{E}(k+1) = \tilde{A}\tilde{E}(k) + \tilde{B}(u(k) + d(k)) + \tilde{B}_a v_a(k) \tag{2.5}$$

where

$$\tilde{E}(k) = (e_w^T(k),\ e^T(k))^T \tag{2.6}$$

$$\tilde{A}(k) = \begin{bmatrix} A_w & B_w & 0 \\ 0 & A_{11} & A_{12} \\ 0 & A_{21} & A_{22} \end{bmatrix},\ \tilde{B}(k) = \begin{bmatrix} 0 \\ B_1 \\ B_2 \end{bmatrix},\ \tilde{B}_a = \begin{bmatrix} 0 \\ B_{a1} \\ B_{a2} \end{bmatrix} \tag{2.7}$$

The FSSMC control law is proposed as

$$u(k) = (\tilde{H}\tilde{B})^{-1}[(1 - qT)s(k) - \tilde{H}\tilde{A}\tilde{E}(k) - (\varepsilon T + \beta)\,sgn(s(k))] \tag{2.8}$$

where $\beta = \tilde{H}\tilde{B}D + \tilde{H}\tilde{B}_a V_a$, $\tilde{H} = [C_w\ D_w\ h_2]$, $q > 0$, $1 - qT > 0$, and $0 \lessgtr \varepsilon < 1$. $s(k)$ defines the sliding dynamics for $\tilde{E}(k)$, and it is yet to be designed. Substituting equation (2.8) into equation (2.2), after some algebra, the approaching dynamics of the system is represented as

$$s(k + 1) = (1 - qT)s(k) - (\varepsilon T + \gamma(k))sgn(s(k)) \tag{2.9}$$

where

$$\gamma(k) = \beta - \tilde{H}\tilde{B}d(k)sgn(s(k)) - \tilde{H}\tilde{B}_a v_a(k)sgn(s(k)) \tag{2.10}$$

with $0 \leq \gamma(k) \leq 2\beta = \gamma$.

3 Stability Analysis

Sliding mode control needs to satisfy two conditions to ensure the stability: (a) Approaching condition: the trajectory $s(k)$, starting from any initial point, reaches to the sliding surface $s(k) = 0$ in finite time; and (b) Sliding condition: after the trajectory reaches the sliding surface, it stays on it. This means that the sliding surface $s(k) = 0$ should define stable dynamics for $\tilde{E}(k)$, which ensures the boundedness of the tracking error $e_1(k)$ and $e_2(k)$ when $s(k)$ is bounded. Therefore, the overall stability analysis for system (2.2) with controller (2.8) includes both the approaching phase and the sliding phase.

3.1 Approaching Phase

This part shows that the sliding surface (switching plane) $s(k) = 0$ will be reached in finite time if the approaching dynamics satisfies equation (2.9). Discrete-time sliding mode control analysis is known to be more complex than the continuous-time case. Gao et al. (1995) proposed several stability conditions for a general class of discrete-time approaching dynamics: (a) starting from any initial point, the trajectory will move monotonically toward the switching plane and cross it in finite time; (b) once the trajectory has crossed the switching plane for the first time, it will cross the plane again in every successive sampling period, resulting in a zigzag motion about the switching plane; and (c) the trajectory stays in a band.

In the following, we prove that under equation (2.9), conditions (a)-(c) are satisfied. That is, $s(k)$ will converge to and stay in the band $[-\Delta,\ \Delta]$, where

$$\Delta = \frac{\varepsilon T + \gamma}{1 - qT} \geq \frac{\varepsilon T + \gamma(k)}{1 - qT} = \Delta(k) > 0 \tag{3.1}$$

From equation (2.9), we have

$$s(k+1) = (1 - qT)|s(k)|sgn(s(k)) - (\varepsilon T + \gamma(k))sgn(s(k))$$
$$= (|s(k)| - \Delta(k))(1 - qT)sgn(s(k))$$

When $|s(k)| > \Delta(k)$, $sgn(s(k+1)) = sgn(s(k))$ and $|s(k+1)| = (|s(k)| - \Delta(k))(1 - qT) < |s(k)|$, which implies that $s(k)$ would move towards the band monotonically; similarly, when $|s(k)| < \Delta(k)$, $sgn(s(k+1)) = -sgn(s(k))$ and $|s(k+1)| = (\Delta(k) - |s(k)|)(1 - qT) < \Delta(k)$, which implies that $s(k)$ will go across the switching plane, change its sign at every step and stay in the band thereafter.

In summary, controller (2.8) can drive system (2.2) towards the sliding surface $s(k) = 0$ with the approaching dynamics (2.9) in finite time, and make it stay in the band $[-\Delta,\ \Delta]$ centered around the sliding surface thereafter. In practical implementation, the discontinuous function sgn is usually replaced by a saturation function $sat(s(k)/\phi)$ to inhibit the chatter phenomenon.

7

3.2 Sliding Phase

To guarantee the stability of the overall system, the convergence of $s(k)$ is not sufficient. In this section, we derive conditions for both $e_1(k)$ and $e_2(k)$ to converge to zero when $s(k)$ converges to zero. Consider first the continuous-time sliding surface $s = 0$, where

$$s = e_f + h_2 e_2 = Q_f\{e_1\} + h_2\dot{e}_1 \tag{3.2}$$

Assume that Q_f has the transfer function realization: $Q_f(p) = B(p)/A(p)$, where $p = \frac{d}{dt}$. Then, the dynamics between s and e_1 is

$$e_1 = \frac{1}{\frac{B(p)}{A(p)} + h_2 p} s \tag{3.3}$$
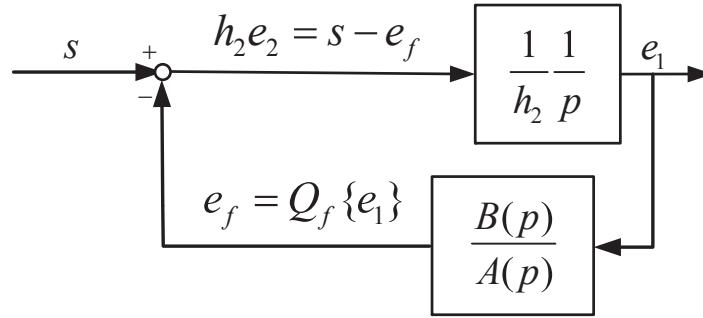
which can be realized by the block diagram in Figure 3.

Figure 3: Dynamics of Sliding Surface

Notice that the open-loop transfer function in Figure 3 is

$$G(p) = \frac{1}{h_2}\frac{B(p)}{A(p)}\frac{1}{p} \tag{3.4}$$

and the closed-loop characteristic equation comes from

$$1 + \frac{1}{h_2}\frac{B(p)}{A(p)}\frac{1}{p} = 0 \tag{3.5}$$

Given $h_2 > 0$, if all of the closed-loop poles are in the left half plane, the systems from s to e_1 and from s to e_2 are stable; thus any bounded s yields bounded e_1 and bounded e_2. We have thus transformed the stability analysis (in sliding phase) into a root-locus problem: as $1/h_2$ changes from 0 to $+\infty$, the poles of (3.3) are on the root loci from the open-loop poles to the open-loop zeros and $-\infty$.

For the discrete-time case,

$$s(k) = e_f(k) + h_2 e_2(k) = Q_f\{e_1(k)\} + h_2 \frac{2}{T}\frac{z-1}{z+1}e_1(k) \tag{3.6}$$

where Q_f has the transfer function realization $Q_f(z) = B_d(z)/A_d(z)$, which is the discretized version of $Q_f(p)$ via Tustin transformation:

$$p = \frac{2}{T}\frac{z-1}{z+1} \tag{3.7}$$

Then the discrete-time dynamics between $s(k)$ and $e_1(k)$ is

$$e_1(k) = \frac{1}{\frac{B_d(z)}{A_d(z)} + h_2 \frac{2}{T}\frac{z-1}{z+1}}s(k) \tag{3.8}$$

and the closed-loop characteristic equation comes from

$$1 + \frac{1}{h_2}\frac{T}{2}\frac{z+1}{z-1}\frac{B_d(z)}{A_d(z)} = 0 \tag{3.9}$$

A root locus analysis similar to the continuous-time case can be performed. Alternatively, noticing that the Tustin transformation preserves stability of the poles and zeros by the mapping of equation (3.7) (where the left-half plane is mapped to the inside of the unit cycle), we can directly conclude that (3.8) is stable if and only if its continuous-time equivalent (3.3) is stable.

4 Filter Design

This section discusses the design of a family of peak filters for FSSMC.

4.1 Peak Filter with Single Peak (PFSP)

A continuous-time PFSP is

$$Q_f(p) = \frac{B(p)}{A(p)} = \frac{p^2 + 2bw_dp + w_d^2}{p^2 + 2aw_dp + w_d^2} \tag{4.1}$$

with $0 < a < b < 1$.

In the following, it will be shown that if $h_2 > 0$, the closed-loop poles of system (3.3) with (4.1) will always be stable; namely, FSSMC has a guaranteed stable sliding surface.
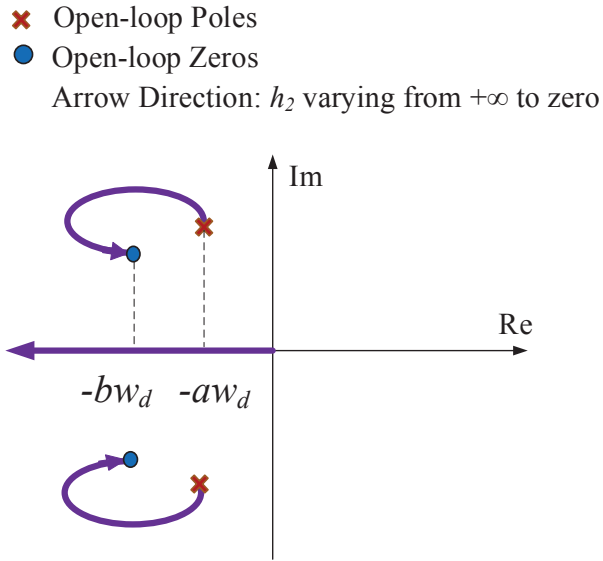

Figure 4: Root Locus with a PFSP

Figure 4 sketches the root loci of the closed-loop system (3.3) with (4.1) as h_2 changes from $+\infty$ to zero, which are always in the left half plane. More specifically, if both the open-loop poles and zeros are in the stable region, a closed-loop pole can never be on the imaginary axes (except the one at origin), or the root loci will never enter the unstable region. To prove this point, suppose there exit such a pole at $p = \gamma j(\gamma \neq 0)$. It must satisfy

$$1 + \frac{1}{h_2}\frac{B(\gamma j)}{A(\gamma j)}\frac{1}{\gamma j} = 0 \tag{4.2}$$

Using (4.1), this means

$$\angle \frac{(w_d^2 - \gamma^2) + 2bw_d\gamma j}{(w_d^2 - \gamma^2) + 2aw_d\gamma j} \frac{1}{\gamma j} = (2n + 1)\pi \tag{4.3}$$

or

$$\arctan \left(\frac{\frac{2bw_d\gamma}{w_d^2 - \gamma^2} - \frac{2aw_d\gamma}{w_d^2 - \gamma^2}}{1 + \frac{2bw_d\gamma}{w_d^2 - \gamma^2} \frac{2aw_d\gamma}{w_d^2 - \gamma^2}} \right) = -\frac{\pi}{2} \tag{4.4}$$

This means that $\left(1 + \frac{2bw_d\gamma}{w_d^2 - \gamma^2} \frac{2aw_d\gamma}{w_d^2 - \gamma^2}\right)$ is 0, which does not take place. The root loci thus will never cross the imaginary axes.

Actually, in the single peak filter case, the sliding surface is a 3rd-order system, and the stability can be directly checked. Combining equation (3.3) and equation (4.1), we have

$$e = \left[\frac{p^2 + 2aw_dp + w_d^2}{h_2p^3 + (1 + 2aw_dh_2)p^2 + (h_2w_d^2 + 2bw_d)p + w_d^2} \right] s \tag{4.5}$$

The closed-loop poles satisfy

$$h_2p^3 + (1 + 2aw_dh_2)p^2 + (h_2w_d^2 + 2bw_d)p + w_d^2 = 0 \tag{4.6}$$

Note that the coefficients $h_2 > 0$, $(1 + 2aw_dh_2) > 0$, $(h_2w_d^2 + 2bw_d) > 0$, $w_d^2 > 0$. From Routh test, the system is stable, if and only if $(1 + 2aw_dh_2)(h_2w_d^2 + 2bw_d) - h_2w_d^2 > 0$, which clearly holds as $(1 + 2aw_dh_2) > 1$ and $(h_2w_d^2 + 2bw_d) > h_2w_d^2$.

In summary, we obtain the strong stability result for FSSMC with a PFSP: as long as both the zeros and poles of (4.1) are stable, the sliding surface will be stable.

The corresponding discrete-time version of (4.1) based on Tustin transformation is

$$Q_f(z) = \frac{B_d(z)}{A_d(z)} \tag{4.7}$$

where $B_d(z) = 4(z-1)^2 + 4Tbw_d(z-1)(z+1) + T^2w_d^2(z+1)^2$, $A_d(z) = 4(z-1)^2 + 4Taw_d(z-1)(z+1) + T^2w_d^2(z+1)^2$. With such a filter, the discrete-time sliding surface described in equation (3.6) is stable if and only if both the zeros and poles of the corresponding continuous-time filter (4.1) are stable.

4.2 Peak Filter with Multi-peaks (PFMP)

Usually there are more than one peak in audio vibrations. Such cases can be handled by FSSMC with a PFMP

$$Q_f(p) = \prod_{i=1}^{n} \frac{B_i(p)}{A_i(p)} \tag{4.8}$$

11

where $B_i(p) = p^2 + 2bw_{di}p + w_{di}^2$, and $A_i(p) = p^2 + 2aw_{di}p + w_{di}^2$. Analogous to previous discussion, a general dynamics between s and e_1 with a PFMP can be represented as

$$e_1 = \frac{1}{\prod_{i=1}^{n} \frac{B_i(p)}{A_i(p)} + h_2 p} s \tag{4.9}$$

and the closed-loop characteristic equation is

$$1 + \frac{1}{h_2} \prod_{i=1}^{n} \frac{B_i(p)}{A_i(p)} \frac{1}{p} = 0 \tag{4.10}$$

Although all the open-loop zeros and poles (except the one at origin) are in the left half plane, the closed-loop root loci may cross the imaginary axes. In this case, the proposed root locus method provides us a way to decide the filter parameters a, b, and the sliding surface parameter h_2 in the p plane. For example, if we would like to design a three-peak filter with $n = 3, a = 0.03, b = 3, w_1 = 900$Hz, $w_2 = 1170$Hz, $w_3 = 2500$Hz, the root locus can be numerically calculated and plotted, as shown in Figure 5. For this particular design, FSSMC always stabilizes the system when $h_2 > 0$. The sliding surface can be further refined by selecting a suitable h_2 based on the transient performance.

For implementation, the equivalent discretized Q_f (by Tustin Transform) is

$$Q_f(z) = \prod_{i=1}^{n} \frac{B_{di}(z)}{A_{di}(z)} \tag{4.11}$$

where $B_{di}(z) = 4(z-1)^2 + 4Tbw_{di}(z-1)(z+1) + T^2 w_{di}^2(z+1)^2$, and $A_{di}(z) = 4(z-1)^2 + 4Taw_{di}(z-1)(z+1) + T^2 w_{di}^2(z+1)^2$. The discrete dynamics between $s(k)$ and $e_1(k)$ is described as

$$e_1 = \frac{1}{\prod_{i=1}^{n} \frac{B_{di}(z)}{A_{di}(z)} + h_2 \frac{2}{T} \frac{z-1}{z+1}} s \tag{4.12}$$

with the closed-loop characteristics equation

$$1 + \frac{1}{h_2} \frac{T}{2} \frac{z+1}{z-1} \prod_{i=1}^{n} \frac{B_{di}(z)}{A_{di}(z)} = 0 \tag{4.13}$$

(4.12) is stable if and only if (4.9) is stable.

In most cases, it is not known in advance at which frequencies the servo performance is most degraded. Such frequency ranges may be identified in real time through processing the error signal $e_1(k)$ by an adaptive notch filter with an adjustable notch frequencies. Some discussions on this are in Chen and Tomizuka (2010, 2012, 2013).
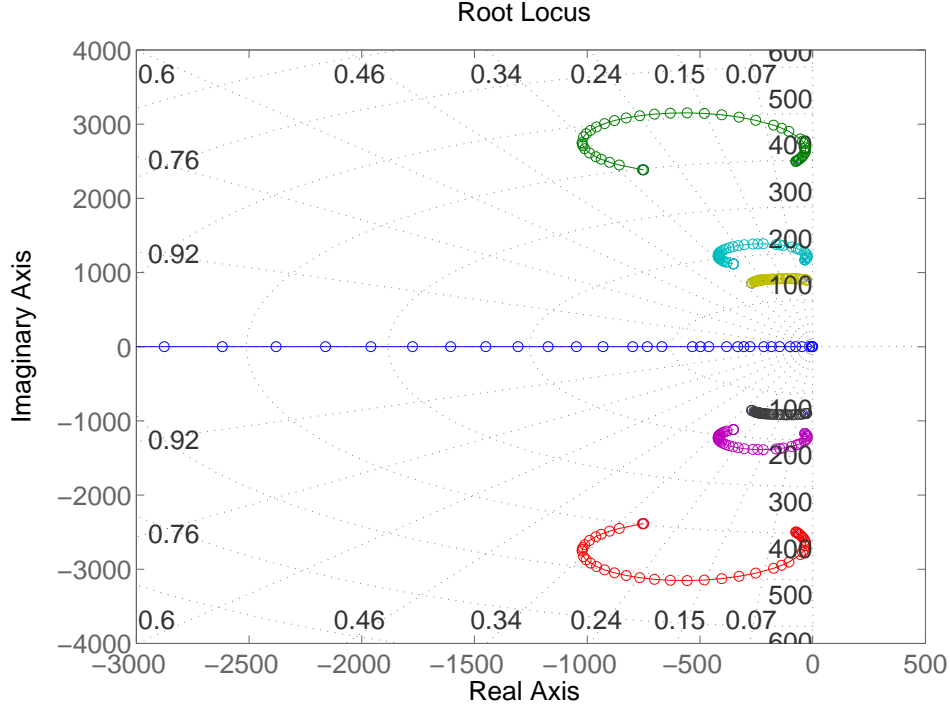
Figure 5: Root Locus with a PFMP

4.3 Frequency Estimation in Filter Design

In most cases, when designing filters, it is unknown around which frequencies the servo performance is degraded, i.e., where PES of HDDs is large. This means that the frequency parameter w_d is unknown. One common identification method for w_d minimizes a specific cost function defined based on the servo performance that we are interested in.

A notch filter Q_n can be introduced to define such a cost function. One notch filter structure is $Q_n = 1/Q_f$. Actually, the selection of Q_n is not limited to $1/Q_f$. For simpler adaptive law design, another kind of notch filter is utilized to identify w_d. For single-peak case, we propose to use

$$Q_n = \frac{z^2 - 2b_n \cos(2\pi\omega_d T)z + b_n^2}{z^2 - 2a_n \cos(2\pi\omega_d T)z + a_n^2}, \tag{4.14}$$

13

where $0 < a_n < b_n < 1$. Denote $e_p = Q_n\{e_1\}$, and $\Omega = \cos(2\pi w_d T)$, then the adaptive law for Ω can be derived through the following optimization problem

$$\min_{\Omega} J = \min_{\Omega} \sum_{1}^{k} \frac{1}{2} e_p^2(i) \tag{4.15}$$

There exit some works on adaptive algorithms for such filters (with both single-peak and multi-peaks): e.g., Chen et al. (1992), Li (1997), Chen and Tomizuka (2010). Note that $0 \le 2\pi w_d T < \pi$, or $0 \le w_d < 0.5/T$. This is the frequency range we can identify based on notch filter (4.14). Figure 6 shows the overall control scheme with identification of w_d.
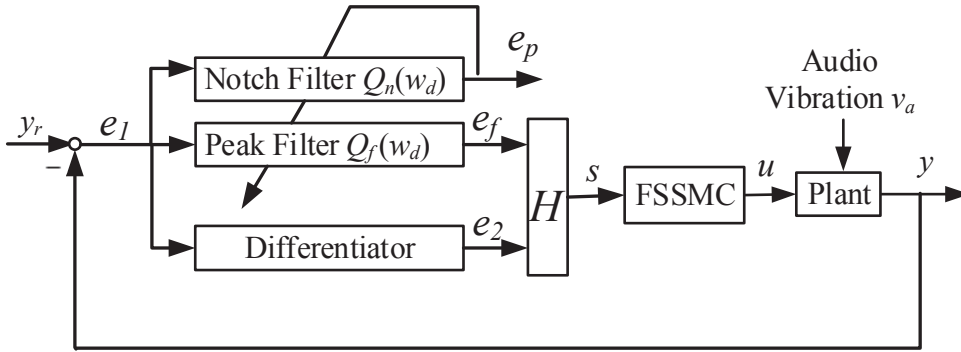

Figure 6: Overall Control Scheme with Adaptive Filter

5 Simulation Results

The proposed frequency-shaped sliding mode control is implemented on the full-order benchmark system in Figure 1. The system parameters are set as follows: rotation speed = 7200 rpm, the number of servo sector = 220, the sampling time $T=3.7879 \times 10^{-5}$ sec, the acceleration constant $k_v=951.2$ m/(s²A), and the position measurement gain $k_y=3.937 \times 10^6$ track·m^{-1}. Three sets of audio vibrations are injected into the plant with peak frequencies around 1200Hz, 900Hz, 2500Hz respectively. Two control algorithms are compared: the traditional sliding mode control without a peak filter, and the proposed frequency shaped sliding mode control. To make the comparison of the two controllers meaningful, all the parameters in the controller such as q (0.1/T) and ε (1×10^{-4}) are set the same.

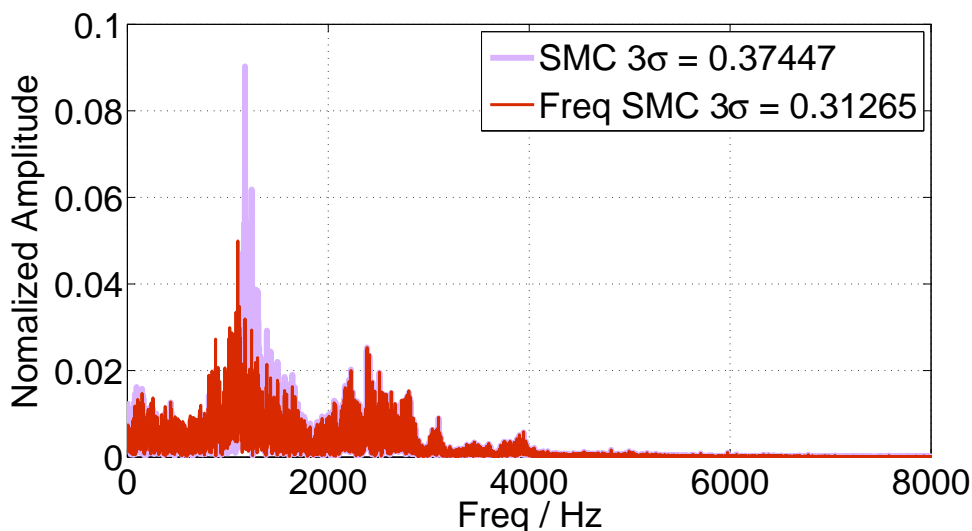

Figure 7: PES Spectrum with Audio Vibration 1

Figures 7 to 9 show the spectrum of PES under the three sets of audio vibrations. The accumulative 3σ value of PES is calculated and shown at the top right corn of each figure. As shown in Figure 7, the accumulative 3σ value of PES has been reduced from 0.37447 to 0.31265 by frequency shaping, approximate 20% reduction; the amplitude reduction around the peak frequency is approximate 50%. Similar results for the other two sets of audio vibrations are shown in Figure 8 (approximate 26% reduction of accumulative 3σ value of PES and 50% amplitude reduction around the peak frequency) and Figure 9 (approximate 13% reduction of accumulative 3σ value of PES and more than 50% amplitude reduction around the peak frequency). Figure 10 provides the 'measured' frequency response plot of the sensitivity function when the excitation is under vibration 3.

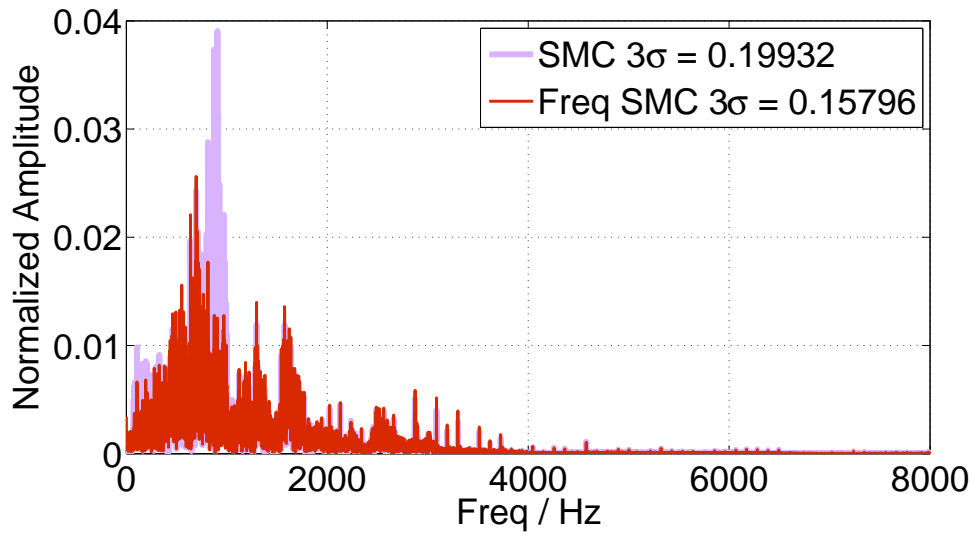In summary, simulation results demonstrate the benefits of the proposed FSSMC: reduc-

15

Figure 8: PES Spectrum with Audio Vibration 2

tion of the overall 3σ value of PES, and reduction of the amplitude of the PES spectrum at specific frequencies, with very small performance sacrifice at other frequencies.
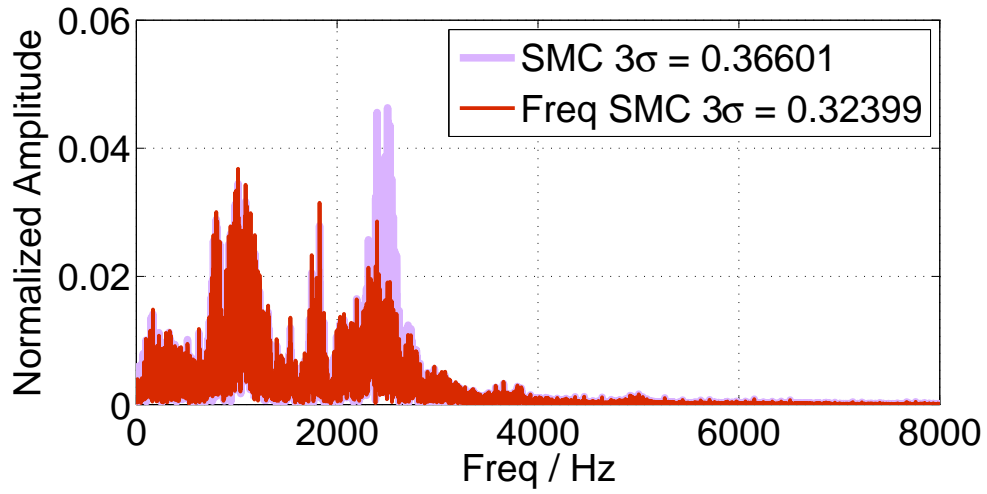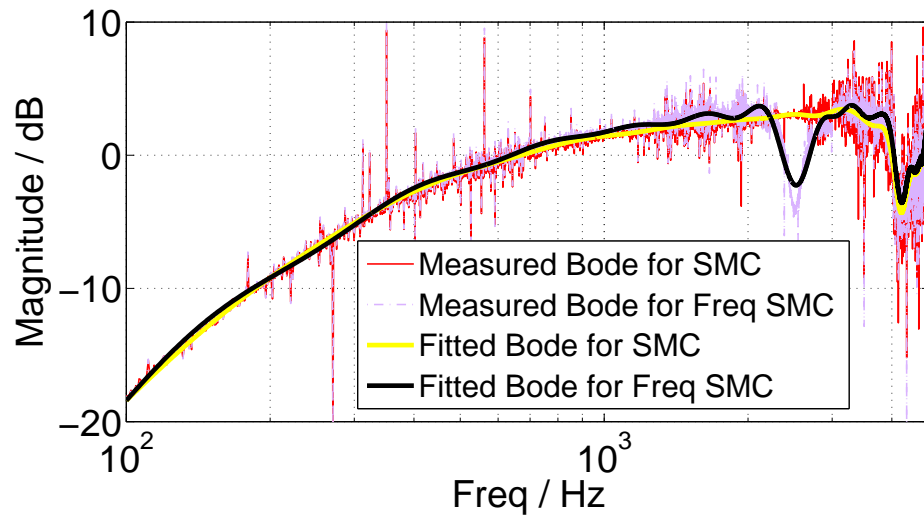
Figure 9: PES Spectrum with Audio Vibration 3

Figure 10: Measured Frequency Response Plot from Vibration 3 to PES

6 Conclusion

This report proposed a frequency-shaped sliding mode control algorithm for the track following of HDDs. It aimed to inhibit high-frequency audio vibrations in the error spectrum. Simulation results validated the benefits of the proposed FSSMC. From the theoretical viewpoint, this report provided stability analysis and a guideline for filter design based on root-locus method, which provides great flexibility and convenience in the frequency-domain controller design. A nice property of the proposed PFSP design is that: as long as both the poles and the zeros of the shaping filter are stable, the sliding surface will be always stable. This property will be used in future work on FSSMC with adaptive shaping filters.

References

Chen, B.-S., Yang, T.-Y., and Lin, B.-H. (1992). Adaptive notch filter by direct frequency estimation. *Signal Processing*, 27(2):161 – 176.

Chen, X. and Tomizuka, M. (2010). Unknown multiple narrow-band disturbance rejection in hard disk drives-an adaptive notch filter and perfect disturbance observer approach. *Proceedings of the 2010 ASME Dynamic Systems and Control Conference, Cambridge, MA*, 1:963–970.

Chen, X. and Tomizuka, M. (2012). A minimum parameter adaptive approach for rejecting multiple narrow-band disturbances with application to hard disk drives. *Control Systems Technology, IEEE Transactions on*, 20(2):408–415.

Chen, X. and Tomizuka, M. (2013). Selective model inversion and adaptive disturbance observer for rejection of time-varying vibrations on an active suspension. In *Control Conference (ECC), 2013 European*, pages 2897–2903.

Gao, W., Wang, Y., and Homaifa, A. (1995). Discrete-time variable structure control systems. *Industrial Electronics, IEEE Transactions on*, 42(2):117–122.

Hu, Q., Du, C., Xie, L., and Wang, Y. (2009). Discrete-time sliding mode control with time-varying surface for hard disk drives. *Control Systems Technology, IEEE Transactions on*, 17(1):175–183.

IEEJ (2007). Ieej technical commitee for novel nanoscale servo control, nss benchmark problem of hard disk drive systems. *http://mizugaki.iis.u-tokyo.ac.jp/nss/*.

Koshkouei, A. and Zinober, A. S. I. (2000). Robust frequency shaping sliding mode control. *Control Theory and Applications, IEE Proceedings* -, 147(3):312–320.

Lee, S.-H., Baek, S.-E., and Kim, Y.-H. (2000). Design of a dual-stage actuator control system with discrete-time sliding mode for hard disk drives. In *Decision and Control, 2000. Proceedings of the 39th IEEE Conference on*, volume 4, pages 3120–3125 vol.4.

Li, G. (1997). A stable and efficient adaptive notch filter for direct frequency estimation. *Signal Processing, IEEE Transactions on*, 45(8):2001–2009.

Mehta, A. and Bandyopadhyay, B. (2009). Frequency-shaped sliding mode control using output sampled measurements. *Industrial Electronics, IEEE Transactions on*, 56(1):28–35.

Moura, J., Roy, R., and Olgac, N. (1997). Frequency-shaped sliding modes: analysis and experiments. *Control Systems Technology, IEEE Transactions on*, 5(4):394–401.

Nonami, K., Ito, T., Kitamura, Y., and Iwabuchi, K. (1996). Frequency-shaped sliding mode control using h_∞ control and μ synthesis theory. In *Variable Structure Systems, 1996. VSS '96. Proceedings., 1996 IEEE International Workshop on*, pages 175–180.

Wu, W. C. and Liu, T. (2005). Frequency-shaped sliding mode control for flying height of pickup head in near-field optical disk drives. *Magnetics, IEEE Transactions on*, 41(2):1061–1063.

Yanada, H. and Ohnishi, H. (1999). Frequency-shaped sliding mode control of an electro-hydraulic servo-motor. *Proceedings of the Institution of Mechanical Engineers, Part I: Journal of Systems and Control Engineering*, pages 441–448.

Young, K. D. and Ozguner, U. (1993). Frequency shaping compensator design for sliding mode. *International Journal of Control*, 57(5):1005–1019.

Zhang, D. Q. and Guo, G. (2000). Discrete-time sliding mode proximate time optimal seek control of hard disk drives. *Control Theory and Applications, IEE Proceedings -*, 147(4):440–446.

Zheng, M., Chen, X., and Tomizuka, M. (2014). Discrete-time frequency-shaped sliding mode control for audio-vibration rejection in hard disk drives. *Proceedings of the 19th IFAC World Congress 2014, Cape Town, South Africa, August 24-29, 2014*, 19:6843–6848.

Zhou, J., Zhou, R., Wang, Y., and Guo, G. (2001). Improved proximate time-optimal sliding-mode control of hard disk drives. *Control Theory and Applications, IEE Proceedings -*, 148(6):516–522.